symmetry

MDPI

Review

Chiral Neuronal Motility: The Missing Link between Molecular Chirality and Brain Asymmetry

Atsushi Tamada

Department of iPS Cell Applied Medicine, Kansai Medical University, Hirakata, Osaka 573-1010, Japan; tamadaat@hirakata.kmu.ac.jp; Tel.: +81-72-804-2632

Received: 18 December 2018; Accepted: 11 January 2019; Published: 16 January 2019

Abstract: Left–right brain asymmetry is a fundamental property observed across phyla from invertebrates to humans, but the mechanisms underlying its formation are still largely unknown. Rapid progress in our knowledge of the formation of body asymmetry suggests that brain asymmetry might be controlled by the same mechanisms. However, most of the functional brain laterality, including language processing and handedness, does not share common mechanisms with visceral asymmetry. Accumulating evidence indicates that asymmetry is manifested as chirality at the single cellular level. In neurons, the growth cone filopodia at the tips of neurites exhibit a myosin V-dependent, left-helical, and right-screw rotation, which drives the clockwise circular growth of neurites on adhesive substrates. Here, I propose an alternative model for the formation of brain asymmetry that is based on chiral neuronal motility. According to this chiral neuron model, the molecular chirality of actin filaments and myosin motors is converted into chiral neuronal motility, which is in turn transformed into the left–right asymmetry of neural circuits and lateralized brain functions. I also introduce automated, numerical, and quantitative methods to analyze the chirality and the left–right asymmetry that would enable the efficient testing of the model and to accelerate future investigations in this field.

Keywords: left–right asymmetry; brain lateralization; cell chirality; growth cone filopodia; neurite growth; actin filaments; myosin V; Riesz transform-differential interference contrast microscopy; structure tensor; optical flow

1. Introduction

In bilateral animals, the body can be divided into left and right parts, which are connected along the midline. Most of the tissues on both sides are equivalent and bilaterally symmetric, but some tissues are asymmetric and not mirror-imaged. Internal organs, such as the heart, liver, pancreas, stomach, and intestines, exhibit obvious asymmetry in shape and location. Compared with the internal organs, the brain appears rather symmetric. From gross anatomical inspection, the brain seems to have two equivalent structures in both hemispheres. However, it is well known that the two hemispheres have different physiological functions. For example, the left hemisphere in humans is specialized for language processing, while the right hemisphere is specialized for certain visuospatial functions [1–3]. The existence of left–right (L–R) brain asymmetry has provoked many fundamental questions among scientists as well as the general public. What are the structural and functional differences between the left and right hemispheres? Why should the left hemisphere be assigned to language and the right to visual functions, not vice versa? How is asymmetry formed during development? Are there common "leftness" and "rightness" features conserved across species? Which anatomical structures and information processing mechanisms underlie the language and visual functions? Are the left and right hemispheres reversible? These crucial questions have yet to be answered. This review aims to provide clues about the answers to these questions, and to shed light on brain asymmetry and its

mechanisms of formation. I start with an overview of our current knowledge on brain asymmetry in humans and non-human animals.

2. Left–Right Brain Asymmetry in Humans

The most evident laterality that all of us are aware of is hand dominance. About 90% of the human population show a dominant use of the right hand [4]. Handedness appears in lateralized thumb sucking behavior during the fetal stages (15 weeks), and is maintained in the later stages (10–12 years) [5,6]. Because the hand is controlled by the motor cortex in the opposite hemisphere, handedness is based on the functional asymmetry of the motor cortices or their upstream areas.

Direct evidence of brain asymmetry in humans has been reported since the nineteenth century. Broca reported that damage to a specific brain region in the left hemisphere is linked to a disability in speech [7]. Succeeding neurological investigations identified the two major language-related brain areas, Broca's and Wernicke's areas in the left hemisphere. More than 95% of right-handers show left hemispheric dominance in language processing, whereas about 70% of left-handers show this dominance [4]. These findings tell us that the laterality of language processing is not strongly linked to handedness.

Many important data on lateralized brain functions were brought from cognitive tests from split-brain patients, whose corpus callosum connecting the two hemispheres was dissected for the treatment of intractable epilepsy [8–10]. Lacking direct information transfer between the hemispheres, these patients exhibited hemispheric functions that were separated from each other. The split-brain studies confirmed that the left hemisphere is dominant for language processing, and found that the right hemisphere has rudimentary language functions. They further revealed specialized functions of the right hemispheres in visuospatial processing. The right hemisphere is superior in various tasks that require part–whole relations, a spatial relationship, motion detection, mental rotation, spatial matching, and mirror-image discrimination [8,10].

The right hemisphere-specific functions have also been revealed by neurological research on patients with hemispheric brain damage. A common symptom after stroke in the right hemisphere is left hemispatial neglect, which is an impairment in attention or response to the stimuli in the left visual field [11]. In contrast, left hemisphere damage rarely causes right hemispatial neglect, but rather, causes aphasia, an impairment of language. Hemispatial neglect can be categorized according to the frame of reference into egocentric neglect, which ignores a half field of body-centered, head-centered, or retinocentric coordinates, and allocentric neglect, which ignores a half portion of the stimuli or objects themselves. A detailed analysis indicates that right-side brain damage usually causes left egocentric neglect, whereas left-side brain damage tends to cause right allocentric neglect, which may have been previously categorized as an inability to read a letter or a word [12]. The laterality could be partly attributed to the difference in the frame of reference or the size of attention. The size dependency in attention and perception was directly tested with composite stimuli containing both larger and smaller features [13]. Left (right) brain-damaged patients exhibit deficits in perception of larger (smaller) features [14]. In healthy humans, attention to larger (smaller) features elicit the neuronal activation in the right (left) hemisphere [15]. These findings suggest that the left (right) hemisphere is specialized for the processing of local (global) features. Another right hemisphere-specific function is facial recognition. Prosopagnosia, a disorder in the perception of familiar faces, is related to a lesion in the fusiform area of the right inferior temporal cortex [16]. The functional asymmetry reported in humans is summarized in Table 1.

In comparison with the wealth of knowledge on functional asymmetry, the structural basis for the L–R brain asymmetry remains unclear. There are some differences in the patterns of gyri and sulci between the two cerebral hemispheres [1,3,17,18]. The most obvious laterality is found in the language-related areas. The left hemisphere has a larger planum temporale and longer Sylvian fissure than the right. Other gross anatomical asymmetries in the brain are known as brain torque and petalia [1,3,17,19]. The right frontal cortex protrudes anterior and the left occipital cortex does so

posterior, generating a counterclockwise (CCW) rotational distortion from the dorsal view, known as brain torque. Distortions of the brain reflect the distortion of the inner surface of the skull, known as the frontal and occipital petalia.

Table 1. Lateralized brain functions and deficits in humans and non-human vertebrates.

Left Hemisphere (Human)	Right Hemisphere (Human)
Right hand control (dominant in 90%)	Left hand control (dominant in 10%)
Language	Visuospatial functions
Aphasia	Left hemispatial neglect
Right allocentric neglect	Left egocentric neglect
Local feature perception	Global feature perception
	Facial recognition
Left Hemisphere (Non-Human Vertebrates)	**Right Hemisphere (Non-Human Vertebrates)**
Vocal communication	Social recognition
Routine behaviors	Emergency behaviors
Discrimination of categorized stimuli	Discrimination of geometric cues
Food searching	Detection and escape from predators
Prey capture	Aggressive behaviors
Local information processing	Global information processing

3. Left–Right Brain Asymmetry in Non-Human Animals

Brain asymmetry is not limited to humans, but is widespread among non-human vertebrates [4,20–23] (Table 1). The gross anatomical asymmetry of Sylvian fissures and the petalia are also found in primates [1]. Microscopic asymmetry is found in the distribution pattern of glutamate receptors in the synapses of the mouse hippocampus [24,25].

Hand preference was reported in non-human primates, but these findings are still controversial [20,26,27]. The direction of asymmetry is not as distinct as the rightward direction in humans, and varies among the species and tasks. Paw or limb preference has been reported in a variety of vertebrates [28], including paw preference in toads [29,30] and footedness in parrots [31].

Although complex language is unique to humans, vocal communication, which is a likely equivalent of language, appears to be commonly localized in the left hemisphere across vertebrate species [4]. Vocal perception is localized to the left hemisphere in macaques [32] and rhesus monkeys [33]. Marmosets dominantly use the right part of the mouth (left hemisphere) in vocalizations [34]. In songbirds, vocalization is dominantly controlled by the nucleus HVC (high vocal center) in the left telencephalon [35]. Intriguingly, lateralization has long since been controversial in the zebra finch, which produces songs with a rich spectro-temporal structure. A recent study reported that the left (right) hemisphere is superior in auditory processing of the temporal (spectral) feature of songs [36], which is consistent with the general directional asymmetry in visual processing [37]. The left hemisphere is dominant for the auditory perception of vocal communication in mice [38] and rats [39]. In frogs, vocalization is controlled by the left hemisphere [40].

Functional laterality in visual perception and visually guided behaviors have been extensively investigated in vertebrate species that have laterally positioned eyes and the complete decussation of optic nerves. In these species, such as birds, frogs, and fish, visual stimuli to the left (right) eye are conveyed to the contralateral right (left) brain hemisphere. The right eye–left hemisphere system is specialized for routine and internally directed behaviors, the discrimination of categorized stimuli, food searching, and prey capture, while the left eye–right hemisphere system is specialized for behaviors in emergency situations, the detection of and escape from predators, spatial behavior using geometric cues, social recognition, and the expression of aggressive behaviors [20–22,41,42]. In functional brain asymmetry, humans and non-human vertebrates seem to share a common pattern of lateralization, suggesting the presence of similar principles conserved across species.

In lower vertebrates, such as fish, amphibians, and reptiles, there are distinct anatomical brain asymmetries in the epithalamus of the diencephalon [43–46]. The sizes of the subnuclei of the habenular nucleus in the epithalamus are different between the two hemispheres. The lateral dorsal subnucleus is larger on the left, while the medial dorsal subnucleus is larger on the right. The parapineal organ is located on the left side. Subsets of afferents from the olfactory bulb innervates the right habenular nuclei [47]. It is uncertain whether the habenular asymmetry is conserved in higher vertebrates.

L–R asymmetry is also seen in the brain and behaviors of invertebrates [48,49]. In the fruit fly, *Drosophila*, a structure called the asymmetrical body is located in the right brain [50]. In the nematode *C. elegans*, some neurons are asymmetric in structural organization, whereas some other neurons are structurally symmetric, but are functional asymmetric with a different molecular expression [51,52].

4. Development of Body Asymmetry

The existence of brain asymmetry in various systems of various species leads to the question of how such asymmetry is formed during development. However, the formation of brain asymmetry is still a puzzle. To get a clue of this mechanism, knowledge on the formation of body asymmetry would be informative. Kartagener syndrome, or primary ciliary dyskinesia, which occurs in one in 10,000–20,000 (0.005–0.01%) humans, is known as a disease with defects in the ciliary functions, caused by immotile cilia, and the reversal of internal organs, called situs inversus [53]. Half of the people with this syndrome show situs inversus and the rest show normal laterality, suggesting that the randomization of asymmetry is the phenotype. Situs inversus is found among vertebrate species, including mice with the *iv* mutation [54].

The body has the following three orthogonal axes: the anterior–posterior (A–P), dorsal–ventral (D–V), and L–R axes (Figure 1). The A–P and D–V axes are determined at the time of fertilization. Then, the L–R axis is defined as the third axis with reference to the A–P and D–V axes. The specification of the L–R axis appears to be a difficult problem, but there should be a mechanism that senses the polarity of the A–P and D–V axes and converts it to the polarity of the L–R axis. Brown and Wolpert proposed a three-step model for the formation of L–R asymmetry [55]. At first, the asymmetry of the molecules is converted into the asymmetry at a cellular level. Next, the cellular asymmetry gives a directional bias on the mechanism of the random generation of asymmetry, so as to favor one direction. Finally, the difference between the two sides are interpreted and used for the differentiation of side-specific structures and tissues.

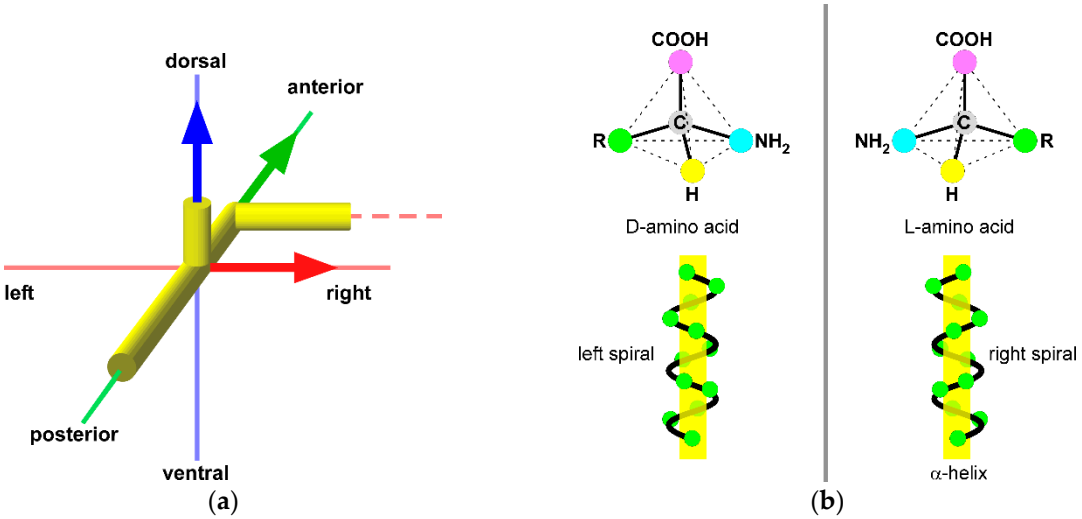

Figure 1. Determination of the left–right axis by molecular chirality. (**a**) Geometric relationship between the three axes; the anterior–posterior (A–P), dorsal–ventral (D–V), and left–right (L–R) axes. A hypothetical chiral "F-molecule" of Brown and Wolpert's model specifies the L–R axis and its polarity. (**b**) Examples of chiral molecules. Amino acids and α-helix polypeptides.

At the step of conversion, a chiral molecule, termed the "F-molecule", is hypothesized to break the symmetry (Figure 1). The F-molecules would be aligned to the A–P and D–V axes, and specify the L–R axis with its direction. As a result, the asymmetry or chirality would be generated at the cellular or multicellular levels. The identity of the F-molecule that determines the body asymmetry is still unclear, but its close association with cytoskeletal elements has been suggested [56].

Many vertebrates use cilia at the node, a transient midline structure formed during gastrulation, for breaking the symmetry [57–59]. The nodal cilia, which are posteriorly tilted [60], rotate counterclockwise (CCW) from the proximal–distal viewpoint, and generate a leftward fluid flow in the node [57]. The nodal cilia and the leftward fluid flow is essential for the determination of the asymmetry [57,58,61]. The posterior tilt of the cilia is regulated via a planar cell polarity (PCP) pathway along the A–P axis [62]. Recent studies revealed that the PCP pathway is controlled by myosin Id in Xenopus and zebrafish [63–65].

The above findings indicate the role of nodal cilia in the formation of asymmetry, but the situation is not so simple. In chicks, a nodal flow is not observed, suggesting the existence of other mechanisms [58,59,66]. There is evidence that symmetry breakage occurs much earlier [67]. The ion flux model and the chromatid segregation model have been proposed as alternative mechanisms [68].

Despite the discrepancy in the symmetry breaking step, the downstream signaling is conserved among the vertebrates. The L–R specification elicits the asymmetric expression of Nodal, a secreted protein of the transforming growth factor beta (TGF-β) superfamily, in the left lateral plate mesoderm [69]. The expression of Nodal triggers the signaling cascade for side-specific organogenesis [58,59,66].

Among the invertebrates, the arthropods are devoid of the nodal cilia and Nodal [70]. In Drosophila, the asymmetry of the internal organs is controlled by the myosin Id and the PCP pathway [71–74]. Intriguingly, the ectopic expression of myosin Id and myosin Ic exhibits counteracting effects on the chiral twist of the cells and the organisms [75]. Further studies on myosin motors, Nodal, and the nodal flow will reveal the unifying or divergent mechanisms of the L–R body asymmetry formation in vertebrates and invertebrates.

5. Brain Asymmetry versus Visceral Asymmetry

Recent advances in our knowledge of body asymmetry formation raise the question of whether brain asymmetry is controlled by the same mechanisms as visceral asymmetry. The linkage between situs inversus and brain asymmetry has been investigated in humans. The brain torque (frontal and occipital petalia) is reversed in situs inversus patients [76–78]. However, handedness is not different between normal and situs inversus subjects [76,79], and neither is the left hemispheric dominance of language function [76,78,80]. One study [77] reported rightward language dominance in the patients, but the number of subjects was small (two out of three). These findings indicate that the brain torque is regulated in the same mechanism as the formation of visceral asymmetry, but that the handedness and laterality of language processing are primarily determined by mechanisms that are different from those for visceral asymmetry. However, some functional brain asymmetry appears to be affected by visceral asymmetry, because situs inversus subjects show atypical cross-lateralization (with normal laterality in some functions but reversed laterality in others) more frequently than the control subjects [81]. Such atypical discordant lateralization results reduced cognitive performance [81] and might receive evolutionary pressure for elimination [81,82].

The mechanisms have also been experimentally investigated in non-human vertebrates. The formation of structural asymmetry in the epithalamus of zebrafish shares mechanisms with the formation of visceral asymmetry [46]. A situs inversus mutation reverses both the visceral asymmetry and epithalamic asymmetry. However, situs inversus does not reverse two lateralized behaviors, the leftward turning bias (use of right eye) upon entering a novel environment and the rightward turning bias (use of left eye) in case of emergency [83], generating atypical lateralization [84]. These findings suggest the presence of alternate mechanisms that are different from those for visceral

asymmetry in zebrafish. Situs inversus mutants also show less adaptation to a novel environment, which might result from this atypical lateralization [83,84]. In *iv* mice, the asymmetric synaptic organization [24,25] is not randomized as the body asymmetry, but shows right isomerism (both hemispheres show the right phenotype) [85].

In birds, it is not known whether visceral laterality controls brain asymmetry, but several studies provide evidence for the non-genetic regulation of lateralized behavior [21–23]. The right eye, which is located near the shell in the egg, receives more light and develops nerve projections faster than the left eye. This bias is considered to produce the lateralized behaviors. These mechanisms in birds cannot be simply applied to mammals, which do not undergo the egg stage during embryogenesis.

6. Chiral Neuronal Motility

The mechanisms of brain asymmetry formation are largely different from those of visceral asymmetry, as discussed above. In the case of the body asymmetry, the chirality at the molecular and cellular levels is critical for the formation of asymmetry. Recently, many studies have demonstrated the existence of chirality at a cellular level [73,86–102]. The cell chirality could be the key intermediate phenotype at the cellular level that bridges the gap between molecular chirality and L–R asymmetry at the tissue or organism levels, which could be also applied to the case of brain asymmetry.

As for the nervous system, Heacock and Agranoff first demonstrated chirality in neurons [86] (Figure 2). They found that explants of goldfish retina extend neurites of optic nerves clockwise (CW), as viewed from above, when they are cultured on glass or plastic surfaces coated with a poly-lysine substrate. The CW neurite growth is a widespread phenomenon observed in various types of neurons or neural tissues in various species, such as the rodent neocortex [88,103], goldfish retinal ganglion cells [104], chick retina, rodent hippocampus [88], and mouse cerebellar granule cells [88]. It is observed on 2D substrates coated with various adhesion molecules, including poly-L (D)-lysine, laminin, N-cadherin, and L1 [88]. The direction of turning is always CW, without exception, although the strength or curvature is dependent on the cell type and the adhesivity to the substrates. The chirality does not depend on gravity or the Coriolis force, which can be easily assessed by the inversion of the culture dish [86]. It is also independent of the magnetic field [86]. The axis of neurite turning can be geometrically defined by the axis of neurite growth and the normal axis of the substrate plane, as the L–R axis is defined by the A–P and D–V axes. In the right-handed system, X-, Y-, and Z-axes point to the direction of neurite growth (distal end), the direction of less adhesivity (or culture medium), and the direction of neurite turning, respectively. The consistent orthogonal relationship between the directions of neurite growth and turning drives the unidirectional circular trajectory of the neurites, and the ratio of their strength determines the curvature and radius of the circle.

CW chiral neurite growth is a robust and universal property that all neurons intrinsically possess, but this phenomenon has long since been neglected by neuroscientists. It may be because such chirality contradicts the general rules for the wiring of neural circuits that are symmetric along the midline [105–107], and is therefore treated as a peculiar artifactual phenomenon. This chirality, however, which geometrically violates the bilateral symmetry, could be a potent source of brain asymmetry.

CW growth is not observed in 3D substrates of collagen gels or collagen films [86,88,108]. The CW turning on 2D substrates is decreased by cytochalasin D, an inhibitor of actin polymerization, but not by paclitaxel, a stabilizer of microtubules, suggesting that the turning is mediated by actin filaments, but not by microtubules [88]. Based on these facts, a model was developed in which the growth cone, a fan-shaped structure located at the tip of a neurite, chirally rotates in the direction that a right-handed screw rotates CW when it advances in the direction of neurite growth (called "right-screw direction"). By testing the hypothesis, it was revealed that the microtubule-rich growth cone body does not rotate, but that the individual filopodia, which are fine needle-like actin-rich processes extending from the growth cone body, autonomously rotate in a right-screw direction [88] (Figure 2). The 3D time-lapse imaging and quantitative kinematic analysis further revealed that the filopodia simultaneously exhibit a retractive treadmill motion and a right-screw rotation, that together generate a left-spiral motion [99].

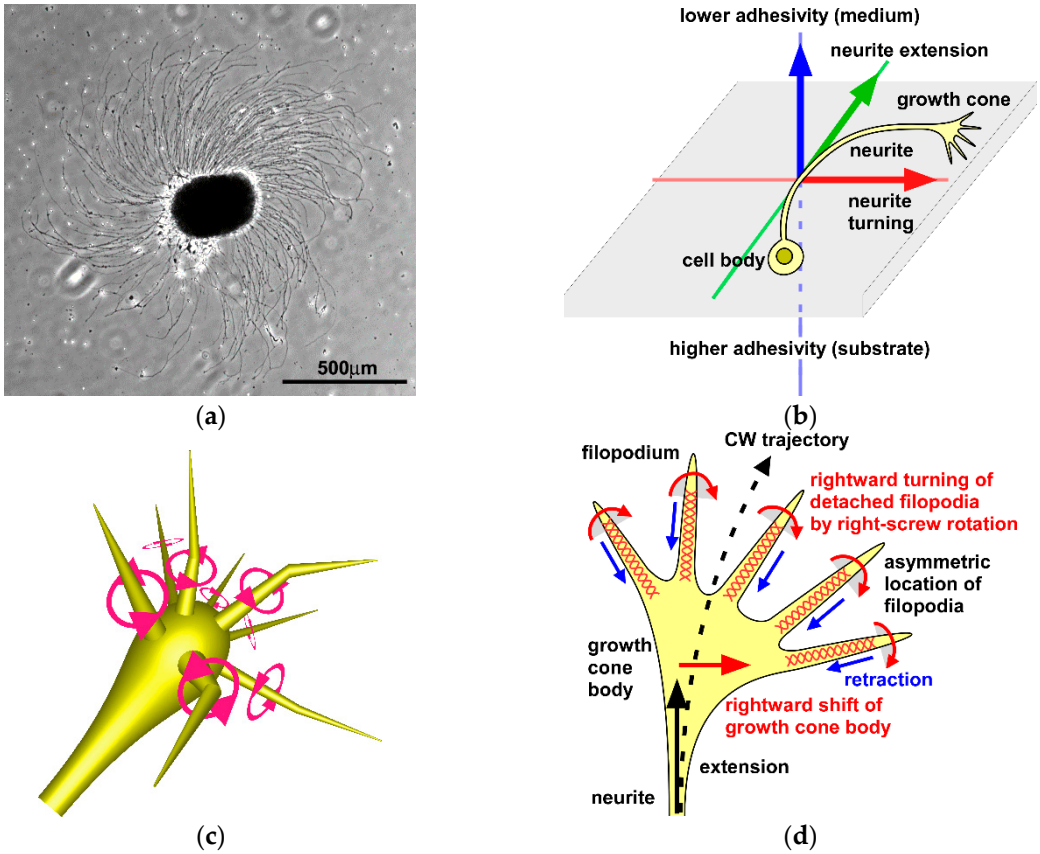

Figure 2. Chiral patterns in neuronal motility. (**a**) Clockwise neurite growth from explants of the mouse hippocampus on a poly-lysine-coated coverslip (top view). (**b**) Geometric relationship between the direction of the neurite extension, the axis of adhesivity (substrate-medium), and the direction of neurite turning. (**c**) Right-screw rotation of growth cone filopodia in 3D substrates. (**d**) Distortion of the growth cone driven by the right-screw filopodial rotation and clockwise turning of the growth cone on 2D substrates. (**d**) Modified from the literature [99] (CC-BY 4.0).

The relationship between the right-screw and left-helical rotation of the growth cone filopodia and the neurite turning behavior dependent on the dimension of the substrates is explained as follows. In homogeneous 3D substrates, the filopodial rotation only causes its axial spin, which does not drive any net biased motion, resulting in the straight migration of the growth cone and the neurite. On 2D substrates, filopodia that adhere to the substrates receive restriction of their lateral motion; but, once detached from the substrates, the filopodia start to rotate in the right screw direction, and attach to the substrates again, but on the right side (as shown by the 2D time-lapse imaging in the literature [88]). These series of motion cause the biased distribution of filopodia on the right side and the rightward twist of the growth cone. The rightward bias of the filopodia causes the rightward traction of the growth cone body [88], driving the circular growth of the neurite. Such differential behaviors in 3D and on 2D substrates represent the extreme cases only found in vitro. The in vivo environments in the brain would be a situation in between 2D and 3D. Heterogenous 3D brain tissues with an anisotropic distribution of adhesion molecules could be an environment similar to 2D substrates for the generation of chiral neuronal growth.

7. Molecular Mechanism Generating Chiral Neuronal Motility

It has been revealed that the chiral motility of growth cone filopodia and growing neurites is driven by interactions between actin filaments and myosin V motors [88]. An actin filament, which is a macromolecule composed of many actin subunits, forms a right-handed double helix with a helical repeat of 36-nm length and 13 subunits (Figure 3). Class V myosin is a dimeric class of the

myosin superfamily that comprises the following three members in vertebrates: myosin Va, Vb, and Vc [109–111]. Myosin Va is a left-handed spiral motor toward the plus end of the actin filaments [112]. Free myosin Va walks along an actin filament with an average step size of 34.8 nm, which is slightly shorter than the helical repeat length, stepping on the 11th or 13th subunits. Stepping on the 13th subunit generates a straight linear motion, whereas stepping on the 11th subunit creates a leftward deviation. In this way, myosin Va exhibits a plus-end-directed left-spiral motion along the actin filament (Video S1, Supplementary Materials). Thus, at a molecular level, the actin filaments show the chiral structure, and the myosin V motors show the chiral motility on the actin filaments.

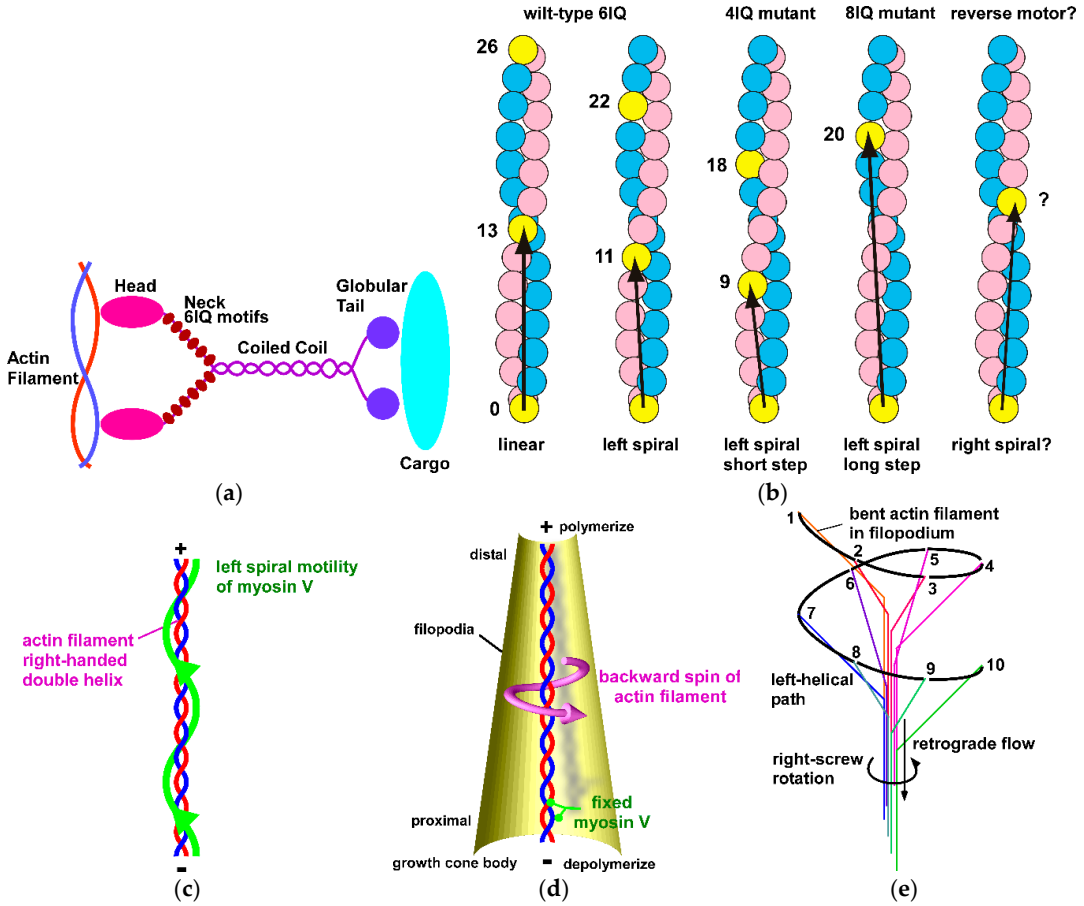

Figure 3. Chiral rotation of filopodia driven by the left-helical myosin V motor. (**a**) Molecular structure of myosin V. (**b**) Stepping patterns of myosin V on actin filaments. Myosin V steps on the 11th or 13th actin subunits, generating a straight or left-spiral motion. 4IQ and 8IQ mutants are predicted to step leftward on the 9th and 20th subunits, respectively. A rightward-stepping motor would generate a left-spiral motion. (**c**) Left-spiral motion of free myosin V on a fixed actin filament. (**d**) Left-helical backward axial spin of an actin filament in a filopodium caused by a fixed myosin V. (**e**) Left-helical twirling of a bent actin filament driven by a retrograde flow and right-screw rotation.

The stepping pattern of myosin V is regulated by the neck domain (Figure 3). The neck domain is composed of six IQ motifs, and functions as a rigid lever arm during walking on actin filaments. It has been shown that the neck length determines the step size [113,114]. Mutant myosin V with four IQ motifs has a shorter step size, whereas that with eight motifs has a larger step size, showing a linear relationship between the neck length and the step size. The 4IQ mutant is predicted to step on the ninth subunit on the left side, and move left-spirally with a steeper angle than the wild type. The step size of the 8IQ mutant is longer than the helical repeat of 36 nm, but it does not seem to show the rightward deviation. The 8IQ mutant is predicted to step on the 20th subunit on the left side of the opposite strand, showing a left-spiral motion. It will be very useful to engineer a mutant myosin V

that exhibits a right-spiral motility. Such molecules would drive a left-screw right-helical rotation of filopodia and CCW neurite growth, and would have the potential to reverse the direction of the L–R brain asymmetry. However, currently, a simple extension of the neck domain does not appear to be sufficient for reversing the helicity of myosin V. There may be a molecular structure in myosin V that prefers leftward stepping to rightward stepping.

Filopodia are composed predominantly of actin filaments that are aligned unidirectionally with their plus end pointing to the tip [115]. Myosin Va colocalizes with both microtubules and actin filaments, but is not enriched in the filopodial actin filaments or accumulated at their distal tips [116], indicating that myosin Va is tethered to some structures like microtubules, without moving freely to the filopodial tips. In such situations, tethered myosin Va would generate a left-helical backward spin of actin filaments (Figure 3; Video S2). This motion itself does not drive net motion of filopodia, but when the actin filaments showed a kinked or bent structure, they would twirl in the right-screw direction or CW, as viewed from the proximal side (Video S3, Supplementary Materials). In this way, the filopodia would rotate in the right-screw direction, which leads to CW neurite growth. Consistent with this notion, the perturbation of myosin Va or Vb, but not myosin Vc, reduced the filopodial rotation and the neurite turning [88]. The differential involvement of the three myosin V members may be due to the processivity (the duration of binding and walking on an actin filament), which is high in myosin Va [117] and myosin Vb [118], but low in myosin Vc [119,120]. Thus, myosin Va and/or myosin Vb is likely to drive the chiral neuronal motility.

8. Role of Chiral Neuronal Motility in Formation of Brain Asymmetry

As discussed in Section 6, the chiral CW neurite growth certainly breaks the bilateral symmetry to some degree. When the chiral neurites are placed on both sides, they would not form mirror-image neuronal connections (Figure 4). However, such obvious asymmetric patterns have not yet been reported in the neuronal projections in vivo. During ontogenesis, neural circuit formation is precisely regulated by a variety of environmental guidance cues [107]. In the context of laterality, midline structures, including the floor plate [105,106], play crucial roles in the formation of crossed and uncrossed projections. They control the laterality by attracting some axons toward the contralateral side and repelling others to keep them on the ipsilateral side. Because such guidance cues regulating laterality are strong during the developmental stages, the intrinsic chiral growth, if any, could be corrected by the overwhelming extrinsic guidance cues. However, the chiral patterns could become evident when the extrinsic cues are lost or attenuated at later or mature stages of development. In such cases, the chiral patterns could be the source of L–R asymmetry.

Here, I discuss the possible chiral patterns in the neurite projections, and their potential contribution to the formation of L–R asymmetric neural circuits in vivo (Figure 4). During development, many axons grow along the A–P or D–V axes [121–123]. For example, commissural crossed axons, which are widely distributed from the forebrain through to the spinal cord, initially grow ventrally along the D–V axis and cross the ventral midline floor plate [107]. If there is differential adhesivity along the apical-basal or ventricle-pia axis, which is orthogonal to both A–P and D–V axes, the ventrally growing axons would receive a CW or CCW bias. In the case of a CW (CCW) bias, the left axons would cross the midline at more posterior (anterior) positions, whereas the right axons would do so at more anterior (posterior) positions. In the case of the uncrossed ipsilaterally projecting axons that initially grow toward the midline, but then turn anterior or posterior, the CW (CCW) bias would increase the posterior (anterior) turning of the left axons and the anterior (posterior) turning of the right axons. In the case of the anteriorly growing axons, the CW (CCW) bias would drive the rightward (leftward) unidirectional turning of the axons on both sides. The above asymmetry is predicted only from the chiral property of the axons and the differential adhesivity of the substrates, without assumption of any L–R biased cues.

If assumption of an L–R difference in adhesivity is allowed, another type of asymmetry could be expected. Assuming that the left hemisphere is more adhesive than the right hemisphere, the left or

right axons would show more circular or straight growth patterns, respectively. As a result, the left circular axons would tend to form recurrent local neural circuits with feedback loops. The right straight axons would follow the environmental guidance cues and tended to form topographic circuits, preserving the global spatial relationship. Such asymmetry in neural circuits could explain the leftness (superiority in local processing) and the rightness (superiority in global processing) that are conserved among the vertebrate species (see Sections 2 and 3). This prediction is not currently supported by evidence. It is not known whether the left and right hemispheres differ in the expression pattern of adhesion molecules. A difference in the circularity of the neural circuits has not yet been reported. A systematic analysis with quantitative methods is required for the detection of the chirality and the L–R asymmetry in neural circuits in vivo.

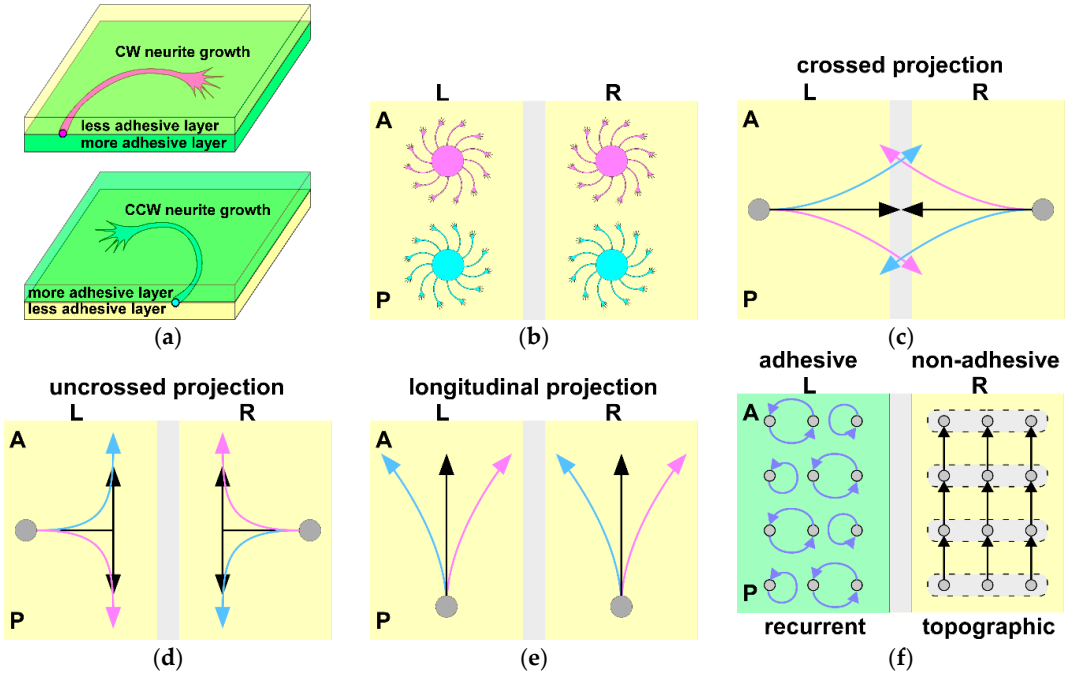

Figure 4. Possible asymmetric neural circuits formed by chiral neuronal motility. (**a**) In the brain, the chiral neurite turning would appear on the plane where the difference or gradient of adhesivity is found, like the boundary of the layers. The direction would be either clockwise (CW) or counter clockwise (CCW). (**b**) The CW or CCW neurites logically break the bilateral symmetry when they are placed on both sides of the brain. (**c**) The commissural axons that are attracted by the midline guidance cues would deviate anteriorly or posteriorly by the intrinsic chirality. (**d**) Uncrossed axons that are repelled by the midline cues and project on the ipsilateral side, would exhibit a lateral bias in the proportion of ascending and descending axons. (**e**) Longitudinally growing axons would receive leftward or rightward unidirectional bias on both sides. (**f**) If there is a side difference in the environmental adhesivity (the left hemisphere is adhesive and the right hemisphere is not adhesive in this extreme case), the right axons would strictly obey the extrinsic guidance cues and form spatially ordered topographic projections, whereas the left axons would tend to exhibit the intrinsic circular patterns that enhance the formation of recurrent local circuits.

9. Methods for Analyzing Chirality and Left–Right Asymmetry

The investigation of L–R brain asymmetry relies on the quantitative analysis of the anatomical differences between the equivalent areas on both sides. However, such an analysis substantially includes several critical problems. An individual shows variability in brain morphology and laterality. Subtle L–R asymmetry at the population level should be discriminated from variances in individual asymmetry. It is also difficult to quantify the morphology of the brain. Some studies use volumetric analysis, which compares the volume of the brain area between the two hemispheres. Such an analysis

is effective for the detection of gross anatomical asymmetry, but cannot detect fine structural differences. Other studies performed an morphometric analysis, which picks up and compares the parameters for the morphological features. However, it is uncertain whether the few arbitrary parameters correctly represent the features, especially in the case of complex morphology. As discussed above, the L–R brain asymmetry is likely related to the chirality and chiral motility of the neurites. If this is the case, then volumetric or morphometric analyses are not effective. An understanding of the chiral structure and chiral motility requires methods that can analyze 3D geometry and 4D motion. In addition, an efficient method for multidimensional imaging is necessary for the acquisition of 3D geometric and 4D motion data. Driven by this necessity, we have recently developed the following three methods, optimized for the analysis of chirality and L–R asymmetry [99].

9.1. Riesz Transform-DIC Microscopy for Less-Toxic Label-Free 3D Time-Lapse Imaging

The analysis of chirality or chiral motion requires 3D or 3D time-lapse (4D) imaging. The most standard method would be fluorescence imaging, but it has difficulties in long-term high-resolution multidimensional imaging, due to the problem of phototoxicity. It cannot be applied to photosensitive fragile structures, such as neuronal growth cones. An alternative is to use less-phototoxic label-free differential interference contrast (DIC) microscopy [124], but it has a problem of a shadow-cast image property along the shear axis of the prism, which hampers 3D visualization and the application of intensity-based analyses. To overcome this difficulty, we invented a novel phase conversion method based on the Riesz transform (RT) [125,126], which is a multidimensional version of the Hilbert transform [127] (Figure 5). This transform, named the composite RT, performs a 90° phase shift along the shear axis, and a 180° phase inversion along the orthogonal axis. DIC microscopy improved with the application of the composite RT, which is called RT-DIC microscopy, enables the acquisition of fluorescence-like intensity images without labeling and generating phototoxicity. Any type of DIC images or a 3D image stack can be easily converted to intensity images or an image stack with an open source ImageJ plugin [99].

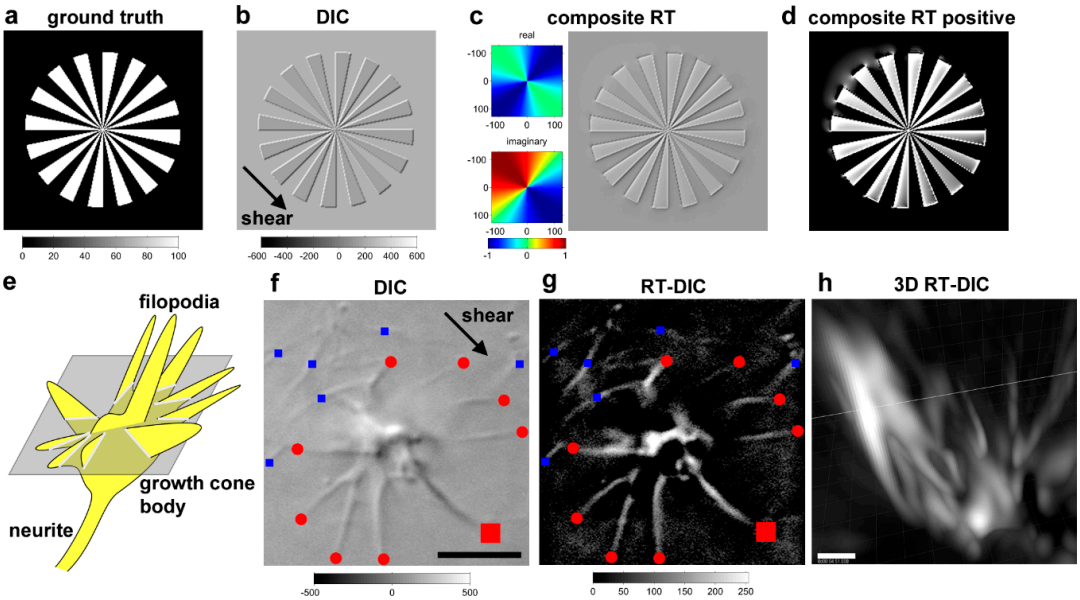

Figure 5. Riesz transform (RT)-differential interference contrast (DIC) microscopy for less-toxic label-free multidimensional imaging. (**a**) A radial grating image for the ground truth. (**b**) DIC image synthesized from (**a**). (**c**) Composite RT (right panel) of (**b**) after passing an RT frequency filter (left panels). (**d**) Thresholding of (**c**) by positive values. (**e**) Schematic of a growth cone for imaging. (**f**) DIC microscopic image of a growth cone. Red and blue dots represent filopodia and collagen fibers, respectively. (**g**) Composite RT of (**f**). (**h**) 3D rendering of z-scanned images of the same growth cone, from oblique view. Modified from the literature [99] (CC-BY 4.0).

9.2. Structure Tensor for Analysis of 3D Morphology

The best and most general way to analyze the morphological features from intensity images, without introduction of any arbitrary morphological parameters, would be to use the structure tensor, or the second moment matrix, which has been frequently used in the field of computer vision [128]. The structure tensor can be calculated by the spatial smoothing of a matrix given by the multiplication of image gradients [99] (Figure 6). The tensor is eigen-decomposed into eigenvectors and eigenvalues, and is further represented as the combination of planar, linear, and spherical tensor bases that are weighed by the corresponding certainty. Thus, the local features around each voxel can be classified into plane, line, and sphere. The eigenvectors with the largest or smallest eigenvalues (the principal or minor eigenvectors) represent the normal orientation of the plane or the orientation of the line, respectively. The voxels constituting the neurites can be detected by the linear certainty. The neurite orientation is represented by the minor eigenvector. The neurite can be tracked by connecting the voxels with the minor eigenvectors. This corresponds to our intuitive perception of the line, by connecting the points with the orientation that image intensity does not change. The curvature of the neurites is represented by the differential of the minor eigenvectors along the arc. The curvature can be used as a parameter for the quantification of the chirality.

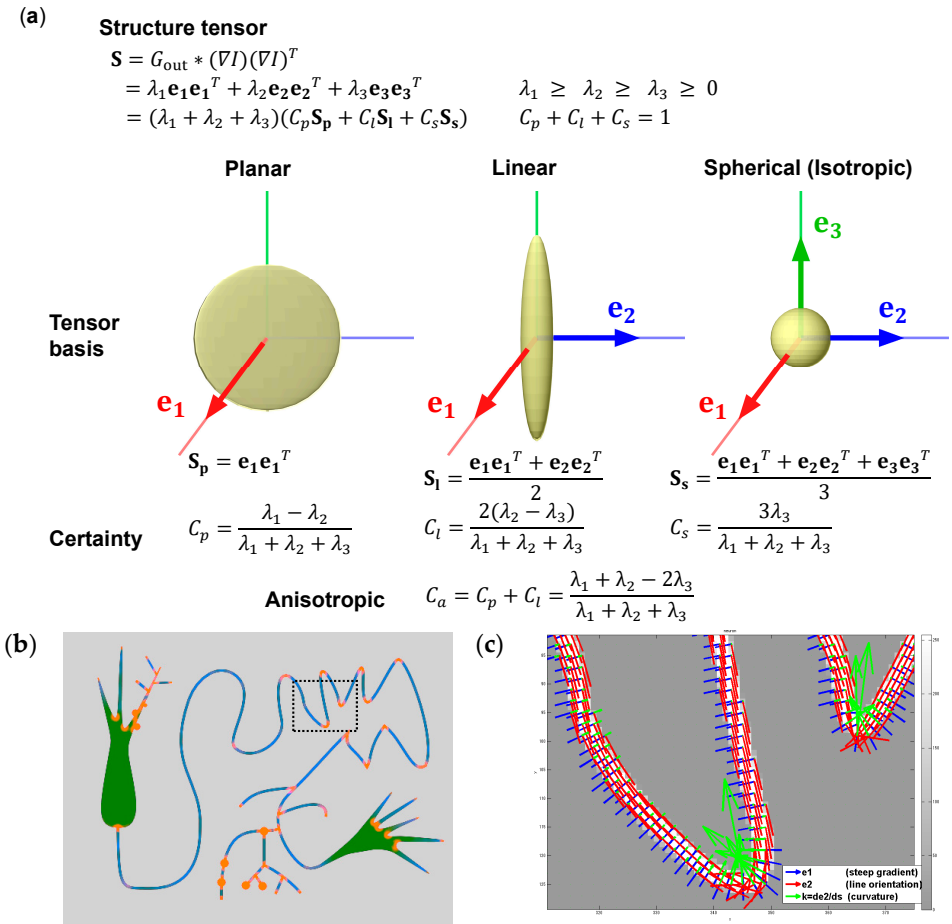

Figure 6. Morphological analysis with structure tensor. (**a**) Shape classification of the structure tensor. Structure tensor is calculated by the Gaussian smoothing (Gout) of a matrix composed of gradients of image intensity *I*. The tensor is decomposed into three tensor bases (planar, linear and spherical bases) and their certainty. Minor eigenvector *e3* and its differential represent fiber orientation and curvature, respectively. (**b**) Feature analysis of a 2D synthetic image of a neuron. λ_1 (blue) and λ_2 (red) are overlaid on the image (green). (**c**) Distribution of principal (blue) and minor (red) orientations, and curvature (green) in dotted rectangle of (**b**). (**a**) is modified from the literature [99] (CC-BY 4.0).

9.3. Optical Flow for Analysis of 3D Motility

The best way to analyze the motility only from multidimensional images would be the optical flow analysis, which also comes from the field of computer vision. The optical flow is the point-wise displacement vector field calculated from two sets of images. We improved the classical 2D optical flow method by Horn and Schunck [129] for 3D image data and for multi-scale estimation [99] (Figure 7). From a series of five time-point image data, four velocity vectors (single-forward, double-forward, single-backward, and double-backward vectors) are calculated from the optical flow. The translational physical quantities (acceleration and jerk) are calculated by the numerical differentiation. rotational physical quantities, including the axes of rotation and the angular velocities (curvature, torsional, and total angular velocities), are calculated from the Frenet–Serret Tangent–Normal–Binormal (TNB) frames. These motion parameters are used for the quantification of the chiral motility, such as rotation and helicity.

Using these three methods, we succeeded in visualization of 4D growth cone motility and automated analysis of the chiral patterns in the morphology and the motility of the growth cones and the growing neurites. We quantified the CW neurite growth and the left-helical motion of growth cone filopodia. Application of these methods further revealed the presence of CW cell migration and right-screw rotation in the cellular slime mold, *Dictyostelium discoideum*, indicating that the cell chirality is an anciently emerged characteristic that is widely observed across phyla [99].

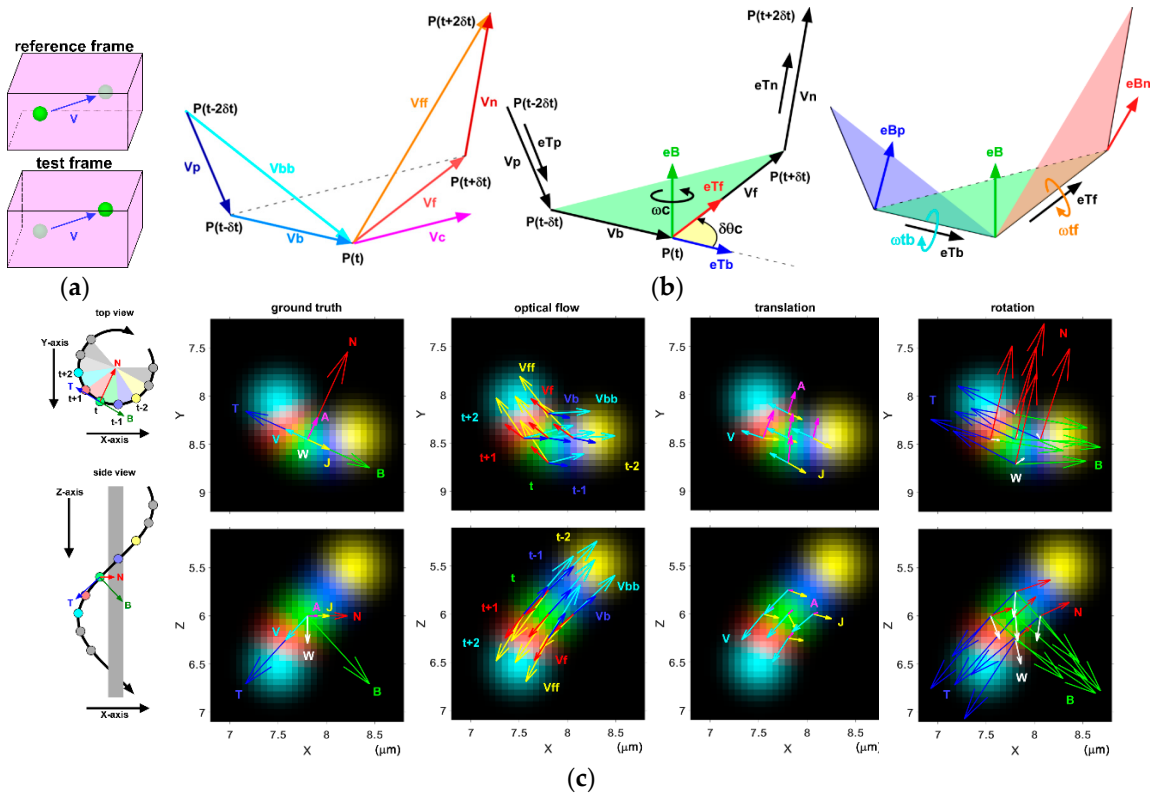

Figure 7. *Cont.*

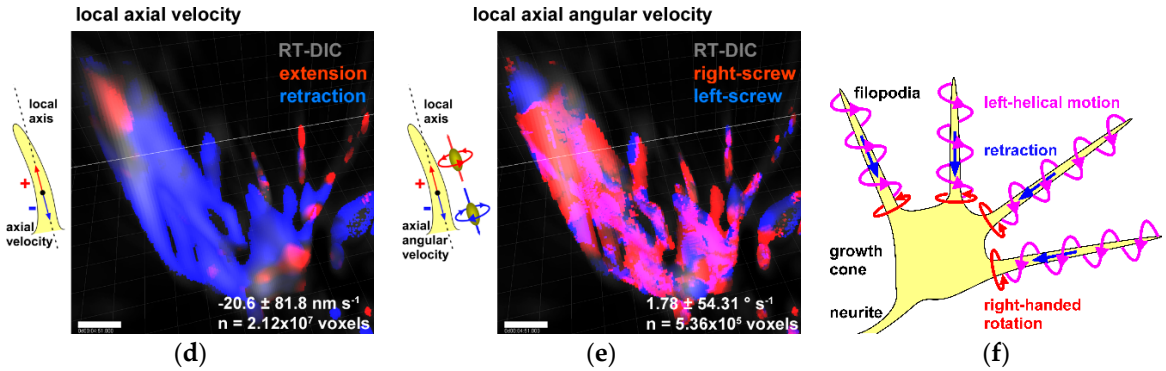

Figure 7. Kinematic analysis with optical flow. (**a**) Optical flow detects voxel-wise displacement or velocity vector fields *V* from two sets of images. (**b**) Calculation of the velocity (left), curvature (middle), and torsional (right) components of the rotation quantities from the four sets of optical flow vector fields. (**c**) Application of kinematic analysis of a right-handed ordinary helical motion of a synthetic sphere. (**d**,**e**) Voxel-wise axial velocity (**d**) and angular velocity (**e**) of neuronal growth cone filopodia. (**f**) Filopodia exhibit a left-helical motion with a retraction and right-screw rotation. Vf, Vff, Vb, and Vbb: single- and double-frame forward and backward optical flow vectors. Vn and Vp: velocity vectors derived from optical flow vectors. Vc: velocity at the central frame. A: acceleration. J: jerk. T, eTf, eTb, eTn, and eTp: tangent unit vectors. N: normal unit vector. B, eB, eBn, and eBp: binormal unit vectors. ωc: curvature angular velocity. Ωtf and ωtb: torsional angular velocity. W: total angular velocity. Modified from the literature [99] (CC-BY 4.0).

10. Conclusions and Future Perspectives

L–R brain asymmetry is a widespread property that is observed among various species. Human and non-human vertebrates seem to share common patterns of functional brain laterality. Evidence suggests that the left hemisphere is specialized for language–vocal functions and local information processing, whereas the right hemisphere is specialized for visuospatial functions and global information processing. The formation mechanisms of brain asymmetry are still unknown, but most of them are independent of those known to underlie body asymmetry. Here, a chiral neuron model is proposed for the formation of brain asymmetry (Figure 8). This model consists of the following steps: (1) molecular chirality of actin filaments and myosin motors generates the right-screw left-helical rotation of neuronal growth cone filopodia; (2) the filopodial rotation drives the CW turning of the neurites on adhesive substrates; (3) the CW neurite growth forms structurally asymmetric neuronal circuits and lateralized brain functions.

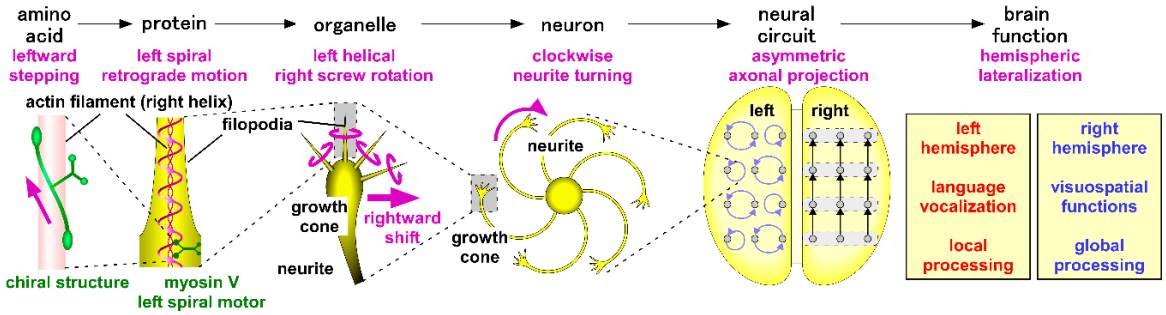

Figure 8. A schematic showing the chiral neuron model for brain asymmetry formation. The molecular chirality of the actin filaments and myosin motors is converted to neuronal chirality in the growth cone motility and neurite growth. In turn, the chiral neuronal motility is hypothesized to construct asymmetric neural circuits that underlie lateralized brain functions.

Currently, step 1 and step 2 have almost been verified, but step 3 is not yet supported by experimental evidence. The most effective way to test this model would be to reverse the functional

brain laterality, by reversing the molecular chirality of actomyosin interactions. The integration of the molecular engineering of myosin motors, genome editing in model animals, cutting-edge imaging techniques, and automated quantitative image analysis would enable model testing and would further the advances in our knowledge of the mechanisms and functions of chirality and L–R brain asymmetry.

Supplementary Materials: The following are available online at http://www.mdpi.com/2073-8994/11/1/102/s1. Video S1: GIF animation showing the left-spiral motility of myosin V on the actin filaments. Video S2: GIF animation showing the left-helical backward spin of the actin filaments by the immobilized myosin V. Video S3: GIF animation showing the left-helical and right-screw twirling of a bent actin filament driven myosin V.

Funding: This research was funded by the Japan Ministry of Education, Sciences, Culture, Sports, and Technology (MEXT) KAKENHI, grant numbers 18H04762 (A.T.) and 18H04730 (Resonance Bio) (A.T.).

Conflicts of Interest: The author declares no conflict of interest.

References

1. Geschwind, N.; Galaburda, A.M. *Cerebral Lateralization: Biological Mechanisms, Associations, and Pathology*; MIT Press: Cambridge, MA, USA, 1987; 283p.
2. Sun, T.; Walsh, C.A. Molecular approaches to brain asymmetry and handedness. *Nat. Rev. Neurosci.* **2006**, *7*, 655–662. [CrossRef]
3. Toga, A.W.; Thompson, P.M. Mapping brain asymmetry. *Nat. Rev. Neurosci.* **2003**, *4*, 37–48. [CrossRef]
4. Corballis, M.C. From mouth to hand: Gesture, speech, and the evolution of right-handedness. *Behav. Brain Sci.* **2003**, *26*, 199–208, discussion 208–260. [CrossRef] [PubMed]
5. Hepper, P.G.; Shahidullah, S.; White, R. Handedness in the human fetus. *Neuropsychologia* **1991**, *29*, 1107–1111. [CrossRef]
6. Hepper, P.G.; Wells, D.L.; Lynch, C. Prenatal thumb sucking is related to postnatal handedness. *Neuropsychologia* **2005**, *43*, 313–315. [CrossRef] [PubMed]
7. Broca, P. Sur le siège de la faculté du langage articulé (15 juin). *Bulletins de la Société Anthropologque de Paris* **1865**, *6*, 377–393. [CrossRef]
8. Gazzaniga, M.S.; Bogen, J.E.; Sperry, R.W. Observations on visual perception after disconnexion of the cerebral hemispheres in man. *Brain* **1965**, *88*, 221–236. [CrossRef]
9. Sperry, R. Some effects of disconnecting the cerebral hemispheres. *Science* **1982**, *217*, 1223–1226. [CrossRef]
10. Gazzaniga, M.S. Forty-five years of split-brain research and still going strong. *Nat. Rev. Neurosci.* **2005**, *6*, 653–659. [CrossRef]
11. Corbetta, M.; Shulman, G.L. Spatial neglect and attention networks. *Annu. Rev. Neurosci.* **2011**, *34*, 569–599. [CrossRef]
12. Kleinman, J.T.; Newhart, M.; Davis, C.; Heidler-Gary, J.; Gottesman, R.F.; Hillis, A.E. Right hemispatial neglect: Frequency and characterization following acute left hemisphere stroke. *Brain Cogn.* **2007**, *64*, 50–59. [CrossRef]
13. Navon, D. Forest before trees: The precedence of global features in visual perception. *Cogn. Psychol.* **1977**, *9*, 353–383. [CrossRef]
14. Robertson, L.C.; Lamb, M.R.; Knight, R.T. Effects of lesions of temporal-parietal junction on perceptual and attentional processing in humans. *J. Neurosci. Off. J. Soc. Neurosci.* **1988**, *8*, 3757–3769. [CrossRef]
15. Fink, G.R.; Halligan, P.W.; Marshall, J.C.; Frith, C.D.; Frackowiak, R.S.; Dolan, R.J. Where in the brain does visual attention select the forest and the trees? *Nature* **1996**, *382*, 626–628. [CrossRef] [PubMed]
16. Gainotti, G.; Marra, C. Differential contribution of right and left temporo-occipital and anterior temporal lesions to face recognition disorders. *Front. Hum. Neurosci.* **2011**, *5*, 55. [CrossRef] [PubMed]
17. Galaburda, A.M.; LeMay, M.; Kemper, T.L.; Geschwind, N. Right-left asymmetrics in the brain. *Science* **1978**, *199*, 852–856. [CrossRef]
18. Van Essen, D.C. A Population-Average, Landmark- and Surface-based (PALS) atlas of human cerebral cortex. *Neuroimage* **2005**, *28*, 635–662. [CrossRef] [PubMed]
19. LeMay, M. Morphological cerebral asymmetries of modern man, fossil man, and nonhuman primate. *Ann. N. Y. Acad. Sci.* **1976**, *280*, 349–366. [CrossRef] [PubMed]
20. Halpern, M.E.; Gunturkun, O.; Hopkins, W.D.; Rogers, L.J. Lateralization of the vertebrate brain: Taking the side of model systems. *J. Neurosci. Off. J. Soc. Neurosci.* **2005**, *25*, 10351–10357. [CrossRef]

21. Rogers, L.; Vallortigara, G. When and Why Did Brains Break Symmetry? *Symmetry* **2015**, *7*, 2181. [CrossRef]
22. Rogers, L.J. A Matter of Degree: Strength of Brain Asymmetry and Behaviour. *Symmetry* **2017**, *9*, 57. [CrossRef]
23. Gunturkun, O.; Ocklenburg, S. Ontogenesis of Lateralization. *Neuron* **2017**, *94*, 249–263. [CrossRef]
24. Kawakami, R.; Shinohara, Y.; Kato, Y.; Sugiyama, H.; Shigemoto, R.; Ito, I. Asymmetrical allocation of NMDA receptor epsilon2 subunits in hippocampal circuitry. *Science* **2003**, *300*, 990–994. [CrossRef] [PubMed]
25. Shinohara, Y.; Hirase, H.; Watanabe, M.; Itakura, M.; Takahashi, M.; Shigemoto, R. Left-right asymmetry of the hippocampal synapses with differential subunit allocation of glutamate receptors. *Proc. Natl. Acad. Sci. USA* **2008**, *105*, 19498–19503. [CrossRef] [PubMed]
26. Andrew, R.J.; Rogers, L.J. The nature of lateralization in tetrapods. In *Comparative Vertebrate Lateralization*; Cambridge University Press: Cambridge, UK, 2002; pp. 94–125.
27. Hopkins, W.D. Chimpanzee right-handedness: Internal and external validity in the assessment of hand use. *Cortex* **2006**, *42*, 90–93. [CrossRef]
28. Rogers, L.J. Lateralization in its many forms, and its evolution and development. *Evol. Hemisph. Spéc. Primates* **2007**, *5*, 23.
29. Bisazza, A.; Cantalupo, C.; Robins, A.; Rogers, L.J.; Vallortigara, G. Right-pawedness in toads. *Nature* **1996**, *379*, 408. [CrossRef]
30. Robins, A.; Lippolis, G.; Bisazza, A.; Vallortigara, G.; Rogers, L.J. Lateralized agonistic responses and hindlimb use in toads. *Anim. Behav.* **1998**, *56*, 875–881. [CrossRef]
31. Harris, L.J. Footedness in parrots: Three centuries of research, theory, and mere surmise. *Can. J. Psychol.* **1989**, *43*, 369–396. [CrossRef]
32. Heffner, H.E.; Heffner, R.S. Temporal lobe lesions and perception of species-specific vocalizations by macaques. *Science* **1984**, *226*, 75–76. [CrossRef]
33. Hauser, M.D.; Andersson, K. Left hemisphere dominance for processing vocalizations in adult, but not infant, rhesus monkeys: Field experiments. *Proc. Natl. Acad. Sci. USA* **1994**, *91*, 3946–3948. [CrossRef] [PubMed]
34. Hook-Costigan, M.A.; Rogers, L.J. Lateralized use of the mouth in production of vocalizations by marmosets. *Neuropsychologia* **1998**, *36*, 1265–1273. [CrossRef]
35. Nottebohm, F. Asymmetries in newral control of vocalization in the canary. In *Lateralization in the Nervous System*; Academic Press: Cambridge, MA, USA, 1977; pp. 23–44.
36. Van Ruijssevelt, L.; Washington, S.D.; Hamaide, J.; Verhoye, M.; Keliris, G.A.; Van der Linden, A. Song Processing in the Zebra Finch Auditory Forebrain Reflects Asymmetric Sensitivity to Temporal and Spectral Structure. *Front. Neurosci.* **2017**, *11*, 549. [CrossRef] [PubMed]
37. Rogers, L.; Koboroff, A.; Kaplan, G. Lateral Asymmetry of Brain and Behaviour in the Zebra Finch, Taeniopygia guttata. *Symmetry* **2018**, *10*, 679. [CrossRef]
38. Ehret, G. Left hemisphere advantage in the mouse brain for recognizing ultrasonic communication calls. *Nature* **1987**, *325*, 249–251. [CrossRef] [PubMed]
39. Fitch, R.H.; Brown, C.P.; O'Connor, K.; Tallal, P. Functional lateralization for auditory temporal processing in male and female rats. *Behav. Neurosci.* **1993**, *107*, 844–850. [CrossRef]
40. Bauer, R.H. Lateralization of Neural Control for Vocalization by the Frog (Rana-Pipiens). *Psychobiology* **1993**, *21*, 243–248.
41. Rogers, L.J. Development and function of lateralization in the avian brain. *Brain Res. Bull.* **2008**, *76*, 235–244. [CrossRef]
42. Vallortigara, G.; Rogers, L.J.; Bisazza, A.; Lippolis, G.; Robins, A. Complementary right and left hemifield use for predatory and agonistic behaviour in toads. *Neuroreport* **1998**, *9*, 3341–3344. [CrossRef]
43. Braitenberg, V.; Kemali, M. Exceptions to bilateral symmetry in the epithalamus of lower vertebrates. *J. Comp. Neurol.* **1970**, *138*, 137–146. [CrossRef]
44. Concha, M.L.; Wilson, S.W. Asymmetry in the epithalamus of vertebrates. *J. Anat.* **2001**, *199*, 63–84. [CrossRef] [PubMed]
45. Aizawa, H.; Amo, R.; Okamoto, H. Phylogeny and ontogeny of the habenular structure. *Front. Neurosci.* **2011**, *5*, 138. [CrossRef] [PubMed]
46. Concha, M.L.; Bianco, I.H.; Wilson, S.W. Encoding asymmetry within neural circuits. *Nat. Rev. Neurosci.* **2012**, *13*, 832–843. [CrossRef] [PubMed]

47. Miyasaka, N.; Morimoto, K.; Tsubokawa, T.; Higashijima, S.; Okamoto, H.; Yoshihara, Y. From the olfactory bulb to higher brain centers: Genetic visualization of secondary olfactory pathways in zebrafish. *J. Neurosci. Off. J. Soc. Neurosci.* **2009**, *29*, 4756–4767. [CrossRef] [PubMed]
48. Frasnelli, E. Brain and behavioral lateralization in invertebrates. *Front. Psychol.* **2013**, *4*, 939. [CrossRef]
49. Frasnelli, E.; Vallortigara, G.; Rogers, L.J. Left-right asymmetries of behaviour and nervous system in invertebrates. *Neurosci. Biobehav. Rev.* **2012**, *36*, 1273–1291. [CrossRef] [PubMed]
50. Pascual, A.; Huang, K.L.; Neveu, J.; Preat, T. Neuroanatomy: Brain asymmetry and long-term memory. *Nature* **2004**, *427*, 605–606. [CrossRef]
51. Hobert, O.; Johnston, R.J., Jr.; Chang, S. Left-right asymmetry in the nervous system: The Caenorhabditis elegans model. *Nat. Rev. Neurosci.* **2002**, *3*, 629–640. [CrossRef]
52. Hobert, O. Development of left/right asymmetry in the Caenorhabditis elegans nervous system: From zygote to postmitotic neuron. *Genesis* **2014**, *52*, 528–543. [CrossRef]
53. Afzelius, B.A. A human syndrome caused by immotile cilia. *Science* **1976**, *193*, 317–319. [CrossRef]
54. Layton, W.M., Jr. Random determination of a developmental process: Reversal of normal visceral asymmetry in the mouse. *J. Hered.* **1976**, *67*, 336–338. [CrossRef] [PubMed]
55. Brown, N.A.; Wolpert, L. The development of handedness in left/right asymmetry. *Development* **1990**, *109*, 1–9. [PubMed]
56. Levin, M.; Mercola, M. The compulsion of chirality: Toward an understanding of left-right asymmetry. *Genes Dev.* **1998**, *12*, 763–769. [CrossRef] [PubMed]
57. Nonaka, S.; Tanaka, Y.; Okada, Y.; Takeda, S.; Harada, A.; Kanai, Y.; Kido, M.; Hirokawa, N. Randomization of left-right asymmetry due to loss of nodal cilia generating leftward flow of extraembryonic fluid in mice lacking KIF3B motor protein. *Cell* **1998**, *95*, 829–837. [CrossRef]
58. Hirokawa, N.; Tanaka, Y.; Okada, Y.; Takeda, S. Nodal flow and the generation of left-right asymmetry. *Cell* **2006**, *125*, 33–45. [CrossRef]
59. Blum, M.; Schweickert, A.; Vick, P.; Wright, C.V.; Danilchik, M.V. Symmetry breakage in the vertebrate embryo: When does it happen and how does it work? *Dev. Biol.* **2014**, *393*, 109–123. [CrossRef] [PubMed]
60. Nonaka, S.; Yoshiba, S.; Watanabe, D.; Ikeuchi, S.; Goto, T.; Marshall, W.F.; Hamada, H. De novo formation of left-right asymmetry by posterior tilt of nodal cilia. *PLoS Biol.* **2005**, *3*, e268. [CrossRef] [PubMed]
61. Nonaka, S.; Shiratori, H.; Saijoh, Y.; Hamada, H. Determination of left-right patterning of the mouse embryo by artificial nodal flow. *Nature* **2002**, *418*, 96–99. [CrossRef] [PubMed]
62. Gray, R.S.; Roszko, I.; Solnica-Krezel, L. Planar cell polarity: Coordinating morphogenetic cell behaviors with embryonic polarity. *Dev. Cell* **2011**, *21*, 120–133. [CrossRef] [PubMed]
63. Tingler, M.; Kurz, S.; Maerker, M.; Ott, T.; Fuhl, F.; Schweickert, A.; LeBlanc-Straceski, J.M.; Noselli, S.; Blum, M. A Conserved Role of the Unconventional Myosin 1d in Laterality Determination. *Curr. Biol.* **2018**, *28*, 810–816. [CrossRef]
64. Juan, T.; Géminard, C.; Coutelis, J.-B.; Cerezo, D.; Polès, S.; Noselli, S.; Fürthauer, M. Myosin1D is an evolutionarily conserved regulator of animal left–right asymmetry. *Nat. Commun.* **2018**, *9*, 1942. [CrossRef]
65. Saydmohammed, M.; Yagi, H.; Calderon, M.; Clark, M.J.; Feinstein, T.; Sun, M.; Stolz, D.B.; Watkins, S.C.; Amack, J.D.; Lo, C.W.; et al. Vertebrate myosin 1d regulates left–right organizer morphogenesis and laterality. *Nat. Commun.* **2018**, *9*, 3381. [CrossRef]
66. McDowell, G.; Rajadurai, S.; Levin, M. From cytoskeletal dynamics to organ asymmetry: A nonlinear, regulative pathway underlies left-right patterning. *Philos. Trans. R. Soc. Lond. B Biol. Sci.* **2016**, *371*. [CrossRef] [PubMed]
67. Levin, M. Left-right asymmetry in embryonic development: A comprehensive review. *Mech. Dev.* **2005**, *122*, 3–25. [CrossRef] [PubMed]
68. Vandenberg, L.N.; Levin, M. A unified model for left-right asymmetry? Comparison and synthesis of molecular models of embryonic laterality. *Dev. Biol.* **2013**, *379*, 1–15. [CrossRef]
69. Levin, M.; Johnson, R.L.; Stern, C.D.; Kuehn, M.; Tabin, C. A molecular pathway determining left-right asymmetry in chick embryogenesis. *Cell* **1995**, *82*, 803–814. [CrossRef]
70. Namigai, E.K.; Kenny, N.J.; Shimeld, S.M. Right across the tree of life: The evolution of left-right asymmetry in the Bilateria. *Genesis* **2014**, *52*, 458–470. [CrossRef] [PubMed]

71. Hozumi, S.; Maeda, R.; Taniguchi, K.; Kanai, M.; Shirakabe, S.; Sasamura, T.; Speder, P.; Noselli, S.; Aigaki, T.; Murakami, R.; et al. An unconventional myosin in Drosophila reverses the default handedness in visceral organs. *Nature* **2006**, *440*, 798–802. [CrossRef]
72. Speder, P.; Adam, G.; Noselli, S. Type ID unconventional myosin controls left-right asymmetry in Drosophila. *Nature* **2006**, *440*, 803–807. [CrossRef]
73. Taniguchi, K.; Maeda, R.; Ando, T.; Okumura, T.; Nakazawa, N.; Hatori, R.; Nakamura, M.; Hozumi, S.; Fujiwara, H.; Matsuno, K. Chirality in planar cell shape contributes to left-right asymmetric epithelial morphogenesis. *Science* **2011**, *333*, 339–341. [CrossRef]
74. Gonzalez-Morales, N.; Geminard, C.; Lebreton, G.; Cerezo, D.; Coutelis, J.B.; Noselli, S. The Atypical Cadherin Dachsous Controls Left-Right Asymmetry in Drosophila. *Dev. Cell* **2015**, *33*, 675–689. [CrossRef] [PubMed]
75. Lebreton, G.; Géminard, C.; Lapraz, F.; Pyrpassopoulos, S.; Cerezo, D.; Spéder, P.; Ostap, E.M.; Noselli, S. Molecular to organismal chirality is induced by the conserved myosin 1D. *Science* **2018**, *362*, 949–952. [CrossRef]
76. Kennedy, D.N.; O'Craven, K.M.; Ticho, B.S.; Goldstein, A.M.; Makris, N.; Henson, J.W. Structural and functional brain asymmetries in human situs inversus totalis. *Neurology* **1999**, *53*, 1260–1265. [CrossRef]
77. Ihara, A.; Hirata, M.; Fujimaki, N.; Goto, T.; Umekawa, Y.; Fujita, N.; Terazono, Y.; Matani, A.; Wei, Q.; Yoshimine, T.; et al. Neuroimaging study on brain asymmetries in situs inversus totalis. *J. Neurol. Sci.* **2010**, *288*, 72–78. [CrossRef] [PubMed]
78. Vingerhoets, G.; Li, X.; Hou, L.; Bogaert, S.; Verhelst, H.; Gerrits, R.; Siugzdaite, R.; Roberts, N. Brain structural and functional asymmetry in human situs inversus totalis. *Brain Struct. Funct.* **2018**, *223*, 1937–1952. [CrossRef] [PubMed]
79. McManus, I.C.; Martin, N.; Stubbings, G.F.; Chung, E.M.; Mitchison, H.M. Handedness and situs inversus in primary ciliary dyskinesia. *Proc. Biol. Sci.* **2004**, *271*, 2579–2582. [CrossRef]
80. Tanaka, S.; Kanzaki, R.; Yoshibayashi, M.; Kamiya, T.; Sugishita, M. Dichotic listening in patients with situs inversus: Brain asymmetry and situs asymmetry. *Neuropsychologia* **1999**, *37*, 869–874. [CrossRef]
81. Vingerhoets, G.; Gerrits, R.; Bogaert, S. Atypical brain functional segregation is more frequent in situs inversus totalis. *Cortex* **2018**, *106*, 12–25. [CrossRef]
82. McManus, C. *Right Hand, Left Hand: The Origins of Asymmetry in Brains, Bodies, Atoms and Cultures*; Harvard University Press: Cambridge, MA, USA, 2004.
83. Barth, K.A.; Miklosi, A.; Watkins, J.; Bianco, I.H.; Wilson, S.W.; Andrew, R.J. fsi zebrafish show concordant reversal of laterality of viscera, neuroanatomy, and a subset of behavioral responses. *Curr. Boil.* **2005**, *15*, 844–850. [CrossRef] [PubMed]
84. McManus, C. Reversed bodies, reversed brains, and (some) reversed behaviors: Of zebrafish and men. *Dev. Cell* **2005**, *8*, 796–797. [CrossRef]
85. Kawakami, R.; Dobi, A.; Shigemoto, R.; Ito, I. Right isomerism of the brain in inversus viscerum mutant mice. *PLoS ONE* **2008**, *3*, e1945. [CrossRef] [PubMed]
86. Heacock, A.M.; Agranoff, B.W. Clockwise growth of neurites from retinal explants. *Science* **1977**, *198*, 64–66. [CrossRef]
87. Xu, J.; Van Keymeulen, A.; Wakida, N.M.; Carlton, P.; Berns, M.W.; Bourne, H.R. Polarity reveals intrinsic cell chirality. *Proc. Natl. Acad. Sci. USA* **2007**, *104*, 9296–9300. [CrossRef]
88. Tamada, A.; Kawase, S.; Murakami, F.; Kamiguchi, H. Autonomous right-screw rotation of growth cone filopodia drives neurite turning. *J. Cell. Biol.* **2010**, *188*, 429–441. [CrossRef] [PubMed]
89. Chen, T.H.; Hsu, J.J.; Zhao, X.; Guo, C.; Wong, M.N.; Huang, Y.; Li, Z.; Garfinkel, A.; Ho, C.M.; Tintut, Y.; et al. Left-right symmetry breaking in tissue morphogenesis via cytoskeletal mechanics. *Circ. Res.* **2012**, *110*, 551–559. [CrossRef]
90. Wan, L.Q.; Chin, A.S.; Worley, K.E.; Ray, P. Cell chirality: Emergence of asymmetry from cell culture. *Philos. Trans. R. Soc.Lond. B Biol. Sci.* **2016**, *371*. [CrossRef]
91. Wan, L.Q.; Ronaldson, K.; Park, M.; Taylor, G.; Zhang, Y.; Gimble, J.M.; Vunjak-Novakovic, G. Micropatterned mammalian cells exhibit phenotype-specific left-right asymmetry. *Proc. Natl. Acad. Sci. USA* **2011**, *108*, 12295–12300. [CrossRef]
92. Naganathan, S.R.; Furthauer, S.; Nishikawa, M.; Julicher, F.; Grill, S.W. Active torque generation by the actomyosin cell cortex drives left-right symmetry breaking. *eLife* **2014**, *3*, e04165. [CrossRef]

93. Sato, K.; Hiraiwa, T.; Maekawa, E.; Isomura, A.; Shibata, T.; Kuranaga, E. Left-right asymmetric cell intercalation drives directional collective cell movement in epithelial morphogenesis. *Nat. Commun.* **2015**, *6*, 10074. [CrossRef]
94. Tee, Y.H.; Shemesh, T.; Thiagarajan, V.; Hariadi, R.F.; Anderson, K.L.; Page, C.; Volkmann, N.; Hanein, D.; Sivaramakrishnan, S.; Kozlov, M.M.; et al. Cellular chirality arising from the self-organization of the actin cytoskeleton. *Nat. Cell. Biol.* **2015**, *17*, 445–457. [CrossRef]
95. Yamanaka, H.; Kondo, S. Rotating pigment cells exhibit an intrinsic chirality. *Genes Cells* **2015**, *20*, 29–35. [CrossRef] [PubMed]
96. Dimonte, A.; Adamatzky, A.; Erokhin, V.; Levin, M. On chirality of slime mould. *Biosystems* **2016**, *140*, 23–27. [CrossRef] [PubMed]
97. Inaki, M.; Liu, J.; Matsuno, K. Cell chirality: Its origin and roles in left-right asymmetric development. *Philos. Trans. R. Soc. Lond. B Biol. Sci.* **2016**, *371*. [CrossRef] [PubMed]
98. Raymond, M.J., Jr.; Ray, P.; Kaur, G.; Singh, A.V.; Wan, L.Q. Cellular and Nuclear Alignment Analysis for Determining Epithelial Cell Chirality. *Ann. Biomed. Eng.* **2016**, *44*, 1475–1486. [CrossRef]
99. Tamada, A.; Igarashi, M. Revealing chiral cell motility by 3D Riesz transform-differential interference contrast microscopy and computational kinematic analysis. *Nat. Commun.* **2017**, *8*, 2194. [CrossRef] [PubMed]
100. Ray, P.; Chin, A.S.; Worley, K.E.; Fan, J.; Kaur, G.; Wu, M.; Wan, L.Q. Intrinsic cellular chirality regulates left-right symmetry breaking during cardiac looping. *Proc. Natl. Acad. Sci. USA* **2018**. [CrossRef]
101. Chin, A.S.; Worley, K.E.; Ray, P.; Kaur, G.; Fan, J.; Wan, L.Q. Epithelial Cell Chirality Revealed by Three-Dimensional Spontaneous Rotation. *Proc. Natl. Acad. Sci. USA* **2018**, *115*, 12188–12193. [CrossRef]
102. Inaki, M.; Sasamura, T.; Matsuno, K. Cell Chirality Drives Left-Right Asymmetric Morphogenesis. *Front. Cell Dev. Biol.* **2018**, *6*, 34. [CrossRef]
103. Romijn, H.J.; Mud, M.T.; Wolters, P.S.; Corner, M.A. Neurite formation in dissociated cerebral cortex in vitro: Evidence for clockwise outgrowth and autotopic contacts. *Brain Res.* **1980**, *192*, 575–580. [CrossRef]
104. Schwartz, M.; Agranoff, B.W. Outgrowth and maintenance of neurites from cultured goldfish retinal ganglion cells. *Brain Res.* **1981**, *206*, 331–343. [CrossRef]
105. Shirasaki, R.; Tamada, A.; Katsumata, R.; Murakami, F. Guidance of cerebellofugal axons in the rat embryo: Directed growth toward the floor plate and subsequent elongation along the longitudinal axis. *Neuron* **1995**, *14*, 961–972. [CrossRef]
106. Tamada, A.; Shirasaki, R.; Murakami, F. Floor plate chemoattracts crossed axons and chemorepels uncrossed axons in the vertebrate brain. *Neuron* **1995**, *14*, 1083–1093. [CrossRef]
107. Yamamoto, N.; Tamada, A.; Murakami, F. Wiring of the brain by a range of guidance cues. *Prog. Neurobiol.* **2002**, *68*, 393–407. [CrossRef]
108. Landreth, G.E.; Agranoff, B.W. Explant culture of adult goldfish retina: Effect of prior optic nerve crush. *Brain Res.* **1976**, *118*, 299–303. [CrossRef]
109. Berg, J.S.; Powell, B.C.; Cheney, R.E. A millennial myosin census. *Mol. Biol. Cell.* **2001**, *12*, 780–794. [CrossRef]
110. Cheney, R.E.; O'Shea, M.K.; Heuser, J.E.; Coelho, M.V.; Wolenski, J.S.; Espreafico, E.M.; Forscher, P.; Larson, R.E.; Mooseker, M.S. Brain myosin-V is a two-headed unconventional myosin with motor activity. *Cell* **1993**, *75*, 13–23. [CrossRef]
111. Rodriguez, O.C.; Cheney, R.E. Human myosin-Vc is a novel class V myosin expressed in epithelial cells. *J. Cell Sci.* **2002**, *115*, 991–1004.
112. Ali, M.Y.; Uemura, S.; Adachi, K.; Itoh, H.; Kinosita, K., Jr.; Ishiwata, S. Myosin V is a left-handed spiral motor on the right-handed actin helix. *Nat. Struct. Biol.* **2002**, *9*, 464–467. [CrossRef] [PubMed]
113. Sakamoto, T.; Wang, F.; Schmitz, S.; Xu, Y.; Xu, Q.; Molloy, J.E.; Veigel, C.; Sellers, J.R. Neck length and processivity of myosin V. *J. Biol. Chem.* **2003**, *278*, 29201–29207. [CrossRef]
114. Sakamoto, T.; Yildez, A.; Selvin, P.R.; Sellers, J.R. Step-size is determined by neck length in myosin V. *Biochemistry* **2005**, *44*, 16203–16210. [CrossRef] [PubMed]
115. Lewis, A.K.; Bridgman, P.C. Nerve growth cone lamellipodia contain two populations of actin filaments that differ in organization and polarity. *J. Cell Biol.* **1992**, *119*, 1219–1243. [CrossRef] [PubMed]
116. Evans, L.L.; Hammer, J.; Bridgman, P.C. Subcellular localization of myosin V in nerve growth cones and outgrowth from dilute-lethal neurons. *J. Cell Sci.* **1997**, *110 Pt 4*, 439–449.
117. Mehta, A.D.; Rock, R.S.; Rief, M.; Spudich, J.A.; Mooseker, M.S.; Cheney, R.E. Myosin-V is a processive actin-based motor. *Nature* **1999**, *400*, 590–593. [CrossRef] [PubMed]

118. Watanabe, S.; Mabuchi, K.; Ikebe, R.; Ikebe, M. Mechanoenzymatic characterization of human myosin Vb. *Biochemistry* **2006**, *45*, 2729–2738. [CrossRef] [PubMed]
119. Watanabe, S.; Watanabe, T.M.; Sato, O.; Awata, J.; Homma, K.; Umeki, N.; Higuchi, H.; Ikebe, R.; Ikebe, M. Human myosin Vc is a low duty ratio nonprocessive motor. *J. Boil. Chem.* **2008**, *283*, 10581–10592. [CrossRef]
120. Takagi, Y.; Yang, Y.; Fujiwara, I.; Jacobs, D.; Cheney, R.E.; Sellers, J.R.; Kovacs, M. Human myosin Vc is a low duty ratio, nonprocessive molecular motor. *J. Boil. Chem.* **2008**, *283*, 8527–8537. [CrossRef] [PubMed]
121. Wilson, S.W.; Ross, L.S.; Parrett, T.; Easter, S.S., Jr. The development of a simple scaffold of axon tracts in the brain of the embryonic zebrafish, Brachydanio rerio. *Development* **1990**, *108*, 121–145. [PubMed]
122. Easter, S.S., Jr.; Ross, L.S.; Frankfurter, A. Initial tract formation in the mouse brain. *J. Neurosci. Off. J. Soc. Neurosci.* **1993**, *13*, 285–299. [CrossRef]
123. Mastick, G.S.; Easter, S.S., Jr. Initial organization of neurons and tracts in the embryonic mouse fore- and midbrain. *Dev. Biol.* **1996**, *173*, 79–94. [CrossRef]
124. Murphy, D.B.; Davidson, M.W. *Fundamentals of Light Microscopy and Electronic Imaging*, 2nd ed.; Wiley-Blackwell: Hoboken, NJ, USA, 2013; 538p.
125. Felsberg, M.; Sommer, G. The monogenic signal. *IEEE Trans. Signal Process.* **2001**, *49*, 3136–3144. [CrossRef]
126. Larkin, K.G.; Bone, D.J.; Oldfield, M.A. Natural demodulation of two-dimensional fringe patterns. I. General background of the spiral phase quadrature transform. *J. Opt. Soc. Am. A Opt. Image Sci. Vis.* **2001**, *18*, 1862–1870. [CrossRef] [PubMed]
127. Gabor, D. Theory of communication. Part 1: The analysis of information. *J. Inst. Electr. Eng. Part III Radio Commun. Eng.* **1946**, *93*, 429–441. [CrossRef]
128. Bigün, J.; Granlund, G. Optimal orientation detection of linear symmetry. In Proceedings of the IEEE First International Conference on Computer Vision (ICCV), London, UK, 8–11 June 1987.
129. Horn, B.K.; Schunck, B.G. Determining optical flow. *Artif. Intell.* **1981**, *17*, 185–203. [CrossRef]